Kinetic Modeling and Test–Retest Reproducibility of ^{11}C-EKAP and ^{11}C-FEKAP, Novel Agonist Radiotracers for PET Imaging of the κ-Opioid Receptor in Humans

Mika Naganawa, Songye Li, Nabeel Nabulsi, Shu-fei Lin, David Labaree, Jim Ropchan, Hong Gao, Michael Mei, Shannan Henry, David Matuskey, Richard E. Carson, and Yiyun Huang

Yale PET Center, Yale University, New Haven, Connecticut

The κ-opioid receptor (KOR) is implicated in various neuropsychiatric disorders. We previously evaluated an agonist tracer, ^{11}C-GR103545, for PET imaging of KOR in humans. Although ^{11}C-GR103545 showed high brain uptake, good binding specificity, and selectivity for KOR, it displayed slow kinetics and relatively large test–retest variability of total distribution volume (V_T) estimates (15%). Therefore, we set out to develop 2 novel KOR agonist radiotracers, ^{11}C-EKAP and ^{11}C-FEKAP. In nonhuman primates, both tracers exhibited faster kinetics than ^{11}C-GR103545 and comparable binding parameters to ^{11}C-GR103545. The aim of this study was to assess their kinetic and binding properties in humans. **Methods:** Six healthy subjects underwent 120-min test–retest PET scans with both ^{11}C-EKAP and ^{11}C-FEKAP. Metabolite-corrected arterial input functions were measured. Regional time–activity curves were generated for 14 regions of interest. One-tissue-compartment and 2-tissue-compartment (2TC) models and the multilinear analysis-1 (MA1) method were applied to the regional time–activity curves to calculate V_T. The time stability of V_T and test–retest reproducibility were evaluated. Levels of specific binding, as measured by the nondisplaceable binding potential (BP_{ND}) for the 3 tracers (^{11}C-EKAP, ^{11}C-FEKAP, and ^{11}C-GR103545), were compared using a graphical method. **Results:** For both tracers, regional time–activity curves were fitted well with the 2TC model and MA1 method (t^* = 20 min) but not with the 1-tissue-compartment model. Given the unreliably estimated parameters in several fits with the 2TC model and a good V_T match between MA1 and 2TC, MA1 was chosen as the appropriate model for both tracers. Mean MA1 V_T was highest for ^{11}C-GR103545, followed by ^{11}C-EKAP and then ^{11}C-FEKAP. The minimum scan time for stable V_T measurement was 90 and 110 min for ^{11}C-EKAP and ^{11}C-FEKAP, respectively, compared with 140 min for ^{11}C-GR103545. The mean absolute test–retest variability in MA1 V_T estimates was 7% and 18% for ^{11}C-EKAP and ^{11}C-FEKAP, respectively. BP_{ND} levels were similar for ^{11}C-FEKAP and ^{11}C-GR103545 but were about 25% lower for ^{11}C-EKAP. **Conclusion:** The 2 novel KOR agonist tracers showed faster tissue kinetics than ^{11}C-GR103545. Even with a slightly lower BP_{ND}, ^{11}C-EKAP is judged to be a better tracer for imaging and quantification of KOR in humans, on the basis of the shorter minimum scan time and the excellent test–retest reproducibility of regional V_T.

Key Words: PET; kinetic modeling; receptor imaging; brain imaging; κ-opioid receptors

J Nucl Med 2020; 61:1636–1642
DOI: 10.2967/jnumed.119.227694

The κ-opioid receptors (KOR) have been implicated in various psychiatric disorders, including addictions, depression, and related mood disorders. We have previously developed and evaluated a set of KOR agonist and antagonist tracers, ^{11}C-GR103545 and ^{11}C-LY2795050, for PET imaging of receptors in humans (*1,2*). The antagonist tracer, ^{11}C-LY2795050, proved to be suitable for imaging and quantifying KOR in the human brain (*3–5*). However, the agonist radiotracer, ^{11}C-GR103545, required a long scan time (140 min) for quantification of binding parameters due to its slow kinetics (*6*). In addition, the variability of outcome measures was higher than desirable (e.g., 15% variability on the total distribution volume [V_T] of the test–retest study (*6*)). Therefore, KOR agonist tracers with faster kinetics and improved imaging properties are needed for reliable quantification of KOR configured in the high-affinity state (*7*). Such agonist tracers are needed to complement the antagonist tracer, which can be used to image and quantify the total KOR levels. We have developed 2 new agonist radiotracers, ^{11}C-EKAP (*8*) and ^{11}C-FEKAP (*9*) (Fig. 1). Evaluation in nonhuman primates showed that they indeed have faster kinetics than ^{11}C-GR103545, with comparable binding specificity. In this paper, we report the first-in-humans evaluation of ^{11}C-EKAP and ^{11}C-FEKAP to establish the appropriate kinetic models for analysis of imaging data and to assess the test–retest reproducibility of binding parameters. The kinetic and binding properties of ^{11}C-EKAP and ^{11}C-FEKAP were also compared with those of ^{11}C-GR103545.

MATERIALS AND METHODS

Human Subjects

Six healthy subjects (20–51 y old; 3 men and 3 women; body weight, 75 ± 13 kg) were enrolled in the study. PET imaging experiments were conducted under a protocol approved by the Yale University School of Medicine Human Investigation Committee and the Yale–New Haven Hospital Radiation Safety Committee and were in accordance with U.S. federal guidelines and regulations for the protection of human research subjects (title 45, part 46, of the *Code of Federal Regulations*). Written informed consent was obtained from all

Received Dec. 19, 2019; revision accepted Mar. 9, 2020.
For correspondence contact: Mika Naganawa, Yale PET Center, Yale University, 801 Howard Ave., P.O. Box 208048, New Haven, CT 06520-8048.
E-mail: mika.naganawa@yale.edu
Published online Mar. 13, 2020.

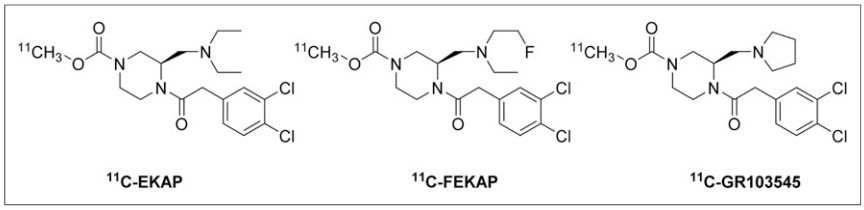

FIGURE 1. Molecular structures of C-EKAP, ^{11}C-FEKAP, and ^{11}C-GR103545.

subjects. All were healthy, as assessed by a physical examination, a comprehensive metabolic panel, a complete blood count, and medical and psychiatric histories. The subjects had no current prescription or illicit drug use, no history of tobacco or nicotine use, no current uncontrolled medical conditions, and no history of neurologic or psychiatric disorders. Women had negative pregnancy tests at intake and on the day of the scans. MR images of all subjects were acquired for verification of no structural brain abnormalities and for PET image registration. MRI was performed on a 3-T whole-body scanner (Trio; Siemens Medical Systems) with a circularly polarized head coil. The dimension and pixel size of MR images were $256 \times 256 \times 176$ voxels and $0.98 \times 0.98 \times 1.0$ mm^3, respectively.

Radiotracer Synthesis

^{11}C-EKAP and ^{11}C-FEKAP were synthesized as previously described (*8,9*). The radiochemical purity of ^{11}C-EKAP and ^{11}C-FEKAP in the final product solution was more than 98%.

PET Imaging Experiments

Each subject underwent 2 PET scans: one with ^{11}C-EKAP and the other with ^{11}C-FEKAP. On the test day, the subjects underwent ^{11}C-EKAP PET first and ^{11}C-FEKAP PET second. On the retest day, the subjects underwent ^{11}C-FEKAP first and ^{11}C-EKAP second, except for 1 subject who underwent the retest scans a week apart. The test and retest scans were 11 ± 11 d apart for ^{11}C-EKAP and 10 ± 8 d apart for ^{11}C-FEKAP, except for 1 subject, who completed the retest scan 69 d after the test scan. All PET scans were conducted on a High Resolution Research Tomograph (Siemens Medical Solutions), which acquires 207 slices (1.2-mm slice separation) with a reconstructed image resolution of about 3 mm. After a 6-min transmission scan for attenuation correction, PET scans were acquired for 120 min in list mode after intravenous administration of ^{11}C-EKAP or ^{11}C-FEKAP over 1 min by an automatic pump (PHD 22/2000; Harvard Apparatus). The injected mass limit was 0.02 μg/kg of body weight. Dynamic scan data were reconstructed into 33 frames (6×0.5 min, 3×1 min, 2×2 min, and 22×5 min) with corrections for attenuation, normalization, scatter, randoms, and dead time using the MOLAR algorithm (a motion-compensation ordered-subsets expectation maximization list-mode algorithm for resolution-recovery reconstruction (*10*)). The reconstruction included event-by-event motion correction (*11*) based on measurements with the Polaris Vicra sensor (NDI Systems), with reflectors being mounted on a swim cap worn by the subject.

Input Function Measurement

The radial artery was catheterized for blood sampling. Manual 0.5-mL samples were collected every 10 s for the first 90 s; thereafter, 21 samples (0.5–10 mL) were collected manually at selected time points. Plasma was obtained by centrifugation at 4°C (2,930*g* for 5 min). Whole blood and plasma were counted in cross-calibrated γ-counters (Wizard 1480 and 2480; PerkinElmer). To reduce noise in the data, the total plasma curve from approximately 5 min onward was fitted to a sum of exponentials.

Plasma Metabolite Analysis

Radioactive metabolites in the arterial plasma were analyzed using a modified automatic column-switching high-performance liquid chromatography method (*12*). Plasma samples collected at 5, 15, 30, 60, and 90 min after injection were mixed with urea (8 M) and then filtered through 1.0-μm Whatman 13-mm GD/X syringe filters (GE Healthcare). Up to 5 mL of plasma filtrate were injected onto the automatic column-switching high-performance liquid chromatography system connected to a capture column (4.6×19 mm) self-packed with Phenomenex Strata-X polymeric solid-phase extraction sorbent and eluting with 1% MeCN in water at 2 mL/min for 4 min. The trapped activity in the capture column was then back flushed and eluted through a Phenomenex Luna C18 phenyl hexyl analytic column (4.6×250 mm, 5 μm) with a mobile phase consisting of 45% MeCN and 55% 0.1 M ammonium formate (v/v) at a flow rate of 1.8 mL/min. High-performance liquid chromatography eluate was fraction-collected and counted in the γ-counters. The fraction counts were corrected for volume and decay. The unmetabolized parent fraction was calculated as the ratio of the sum of radioactivity in fractions containing the parent compound to the total amount of radioactivity collected and was fitted to an integrated γ-function (4 fitted parameters: *a, b, c,* and *d*):

$$f(t) = a \times \left(1 - \int_0^{ct} \exp(-u)u^{d-1}\mathrm{d}u \Big/ \int_0^{\infty} \exp(-u)u^{d-1}\mathrm{d}u\right).$$

In addition, the time-varying extraction efficiency of radioactivity in filtered plasma samples was determined and normalized to that of reference plasma sample. The plasma input function was obtained as the product of the total plasma activity, the parent fraction, and the normalized extraction efficiency.

Measurement of Tracer Free Fraction in Plasma

Arterial blood samples were taken immediately before tracer injection for analysis of the plasma free fraction (f_P). An ultrafiltration method (Centrifree micropartition device 4104A; Millipore) was used for measuring the f_P of tracer in plasma in triplicate. The f_P was determined from the count ratio of ultrafiltrate to plasma.

Image Registration and Definition of Regions of Interest

Regions of interest were defined in the automated anatomic labeling for SPM2 (*13*) in Montreal Neurologic Institute space (*14*). After hardware motion correction, the dynamic PET images were coregistered to the early summed PET images from 0 to 10 min after injection using a 6-parameter mutual information algorithm (*15*) (FMRIB's Linear Image Registration Tool; Functional Magnetic Resonance Imaging of the Brain [FMRIB] Software Library) to eliminate any residual motion. The summed PET image was then coregistered to the individual subject's T1-weighted 3-T MR image (6-parameter rigid registration) and then coregistered to the automated anatomic labeling template in Montreal Neurologic Institute space using a nonlinear transformation (Bioimage suite) (*16*). Using the combined transformations from the template to the individual subject's PET space, regional time–activity curves were generated for 14 regions of interest: amygdala, caudate, centrum semiovale, cerebellum, anterior cingulate cortex, frontal cortex, globus pallidus, hippocampus, insula,

TABLE 1
Subject Information and PET Scan Parameters

Parameter	^{11}C-EKAP			^{11}C-FEKAP		
	Test	Retest	*P*	Test	Retest	*P*
Injected dose (MBq)	625 ± 85	534 ± 121	0.07	447 ± 180	519 ± 223	0.38
Molar activity at time of injection (MBq/nmol)	244 ± 63	205 ± 84	0.35	188 ± 119	237 ± 126	0.43
Injected mass (μg)*	1.15 ± 0.31	1.20 ± 0.35	0.71	1.21 ± 0.39	1.03 ± 0.32	0.34
f_P	24.6% ± 2.8%	24.5% ± 3.1%	0.96	6.3% ± 0.9%	6.2% ± 0.8%	0.73

*Mass limit, 0.02 μg/kg.
n = 6/group.

occipital cortex, posterior cingulate cortex, putamen, temporal cortex, and thalamus.

Quantitative Analysis

The outcome measures were derived with kinetic analysis of the regional time–activity curves using the arterial plasma input function. V_T (*17*) was calculated using 1- and 2-tissue compartment (1TC and 2TC, respectively) models and the multilinear analysis-1 (MA1) method (*18*). The test scans (n = 6) were used for kinetic model assessment. The time stability of V_T estimates was assessed by comparing V_T from shortened scans (ranging from 110 to 50 min) to the 120-min V_T using the MA1 (t^* = 20 min) model. The ratio of V_T from the shortened scan to that from the 120-min scan was computed for each region of interest and duration. Two criteria were adopted to determine a minimum scan duration (*19*): The first criterion was that the average of the ratio was between 0.95 and 1.05. The second criterion was that the interindividual SD of the ratio was less than 0.1. All modeling was performed with in-house programs written with Interactive Data Language (version 8.0; ITT Visual Information Solutions). For parameter estimation, data points were weighted on the basis of the noise-equivalent counts in each frame. Percentage SE (%SE) was estimated from the theoretic parameter covariance matrix. %SE was used to examine the reliability of individual fits (fits were considered unreliable when %SE of V_T was >10%).

Because KOR is distributed throughout the brain, no reference region was available. To predict which KOR radiotracer will show higher specific binding signals, the graphical method of Guo et al. (Guo plot) (*20*) was applied to compare ^{11}C-EKAP and ^{11}C-FEKAP with ^{11}C-GR103545. The equation for the Guo plot to compare tracer A and tracer B is...

$$\mathbf{V}_T^B = \frac{f_P^B}{f_P^A}\frac{K_D^A}{K_D^B}\mathbf{V}_T^A + V_{ND}^B\left(1 - \frac{BP_{ND}^B}{BP_{ND}^A}\right).$$

When plotting $\mathbf{V}_T{}^B$ (y-axis) against $\mathbf{V}_T{}^A$ (x-axis), the sign of the y-intercept predicts which tracer will produce a bigger BP_{ND}. The mean V_T across test scans for ^{11}C-EKAP and ^{11}C-FEKAP and the mean V_T from a previous study (*6*) for ^{11}C-GR103545 were used for the Guo plot. The regression line was estimated with the total least-squares method using weights that are proportional to the inverse of intersubject SD. The relative BP_{ND} can be estimated from the measured intercept if the V_{ND} of tracer B is known.

For the test–retest data, results were evaluated according to 3 criteria: relative test–retest variability (TRV), absolute TRV (aTRV), and intraclass correlation coefficient (ICC). The test and retest scans that were more than 1 mo apart (n = 1) were excluded. TRV was calculated as the difference between the parameters in the test and retest scans divided by their average. The mean of TRV denotes the presence of a trend between the 2 scans, and the SD of TRV is an index of the variability in the difference of 2 estimates. aTRV is the absolute value of TRV and comparable to the error in a single measurement.

RESULTS

Injection Parameters and Plasma Analysis

The mean (±SD) of the administered mass of ^{11}C-EKAP and ^{11}C-FEKAP was 1.18 ± 0.32 μg (range, 0.80–1.65 μg) and 1.12 ± 0.35 μg (range, 0.62–1.61 μg), respectively. The mean administered activity of ^{11}C-EKAP and ^{11}C-FEKAP was 580 ± 111 MBq (range, 382–746 MBq) and 483 ± 197 MBq (range, 152–730 MBq), respectively. There were no adverse or clinically detectable pharmacologic effects in any of the 6 subjects. No significant changes in vital signs or the results of laboratory studies were observed.

Table 1 lists the injected radioactivity dose, molar activity at the time of injection, injected mass, and f_P. There were no significant differences in injected dose, injected mass, or f_P between the test and retest scans with either tracer. Figure 2 displays the parent fractions and metabolite-corrected plasma curves from the test–retest study for both tracers. The parent fractions were similar between the test and retest scans for both tracers. ^{11}C-FEKAP displayed a lower parent fraction than ^{11}C-EKAP in plasma. The mean parent fractions at 60 min after injection were 32% ± 7% and 34% ± 6% for the test and retest scans with ^{11}C-EKAP and 23% ± 5% and 21% ± 5% for the test and retest scans with ^{11}C-FEKAP. However, the actual parent radioactivity levels of the 2 tracers were quite similar (Figs. 2C and D), suggesting that the difference in parent fraction was due to different clearance rates for the radiolabeled metabolites. The f_P was 0.25% ± 0.03% for ^{11}C-EKAP (n = 12) and 0.06% ± 0.01% for ^{11}C-FEKAP (n = 12).

Modeling Results

Radioactivity distribution in the brain was heterogeneous, and the distribution pattern was similar between ^{11}C-EKAP and ^{11}C-FEKAP (Fig. 3). Regional time–activity curves for representative brain regions are shown in Figure 3. The time–activity curves peaked at about 20 and 40 min after injection of ^{11}C-EKAP and ^{11}C-FEKAP, respectively (Fig. 4). Typical examples of curve fittings with 1TC and 2TC models and MA1 are also shown in Figure 4. Regional time–activity curves were fitted well with the

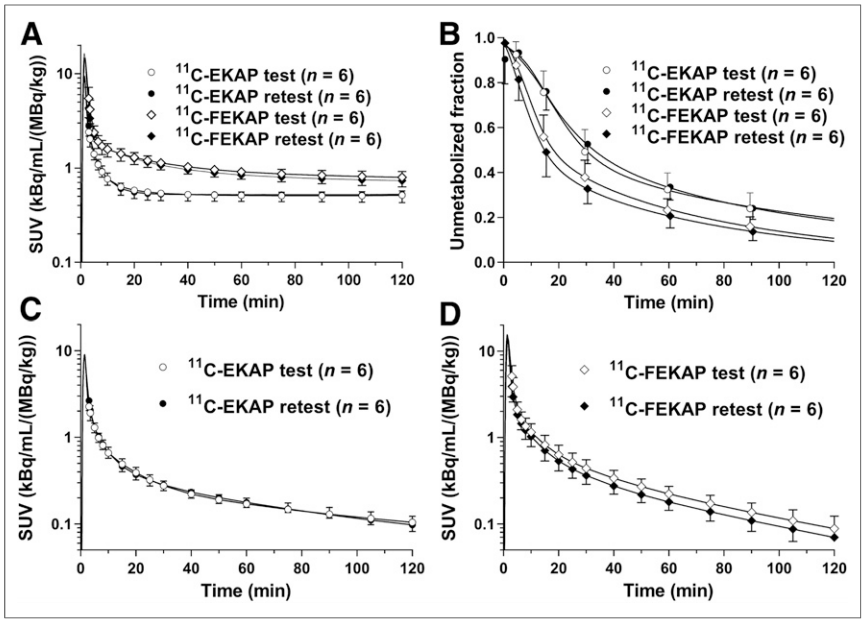

FIGURE 2. Mean ± SD of total plasma activity (A), parent fraction in plasma (B), metabolite-corrected plasma activity over time after injection of ^{11}C-EKAP (C), and metabolite-corrected plasma activity over time after injection of ^{11}C-FEKAP (D). SUV is [concentration/(injected dose/body weight)].

2TC and MA1 models, and to a lesser extent with the 1TC model. The parameters of the 2TC model were not reliably estimated (%SE $>$ 10% in V_T) in a few cases, especially in the amygdala. Given the low ICC of MA1 V_T for ^{11}C-EKAP in the amygdala, quantification was still difficult in the amygdala even with MA1, because of the combination of the small region-of-interest size and slow kinetics. Mean K_1 (mL/cm^3/min) in the 1TC model ranged from 0.09 (centrum semiovale) to 0.21 (putamen) for ^{11}C-EKAP and from 0.033 (centrum semiovale) to 0.076 (insula) for ^{11}C-FEKAP. There were excellent correlations in V_T between the kinetic models (^{11}C-EKAP: $V_{T(1TC)} = 0.96 \times V_{T(2TC)} - 0.53$, $R^2 = 0.98$, and $V_{T(MA1,\ t^* = 20\ min)} = 1.02 \times V_{T(2TC)} - 0.28$, $R^2 = 0.98$; ^{11}C-FEKAP: $V_{T(1TC)} = 0.92 \times V_{T(2TC)} - 0.17$, $R^2 = 0.98$, and $V_{T(MA1,\ t^* = 20\ min)} = 1.02 \times V_{T(2TC)} + 0.11$, $R^2 = 1.00$). These comparisons were performed for the regions with good identifiability, that is, %SE of $V_T < 10\%$ with the 2TC model. For both tracers, t^* for MA1 was selected as 20 min by comparing the MA1 V_T with 2TC V_T. On the basis of the good and consistent quality of fit and comparison with 2TC V_T, the MA1 model was chosen for both tracers.

Regional V_T estimated using 1TC, 2TC, and MA1 ($t^* = 20$ min) and the minimum scan time for the MA1 model is summarized in Table 2. For both ^{11}C-EKAP and ^{11}C-FEKAP, a high V_T was seen in the amygdala, insula, and anterior cingulate cortex, and a lower V_T was seen in the centrum semiovale, cerebellum, and thalamus. The intersubject V_T variability was higher for ^{11}C-FEKAP (MA1, 23%–39%) than ^{11}C-EKAP (MA1, 14%–26%). The minimum scan durations to obtain a stable V_T were 90 and 110 min for ^{11}C-EKAP and ^{11}C-FEKAP, respectively.

Test–Retest Reproducibility

The aTRV of MA1 V_T estimates was good (4%–8%) for ^{11}C-EKAP across all regions except the amygdala (17%) (Table 3). The aTRV of ^{11}C-FEKAP V_T was higher in all regions (13%–26%) than was the aTRV of ^{11}C-EKAP. The test–retest reproducibility of V_T measured by ICC was excellent (0.78–0.98) for ^{11}C-EKAP in all regions except the amygdala (0.19). The ICC of ^{11}C-FEKAP was also generally good (0.63–0.83) except in 3 regions: anterior cingulate cortex (0.57), cerebellum (0.47), and thalamus (0.55).

Comparison of ^{11}C-EKAP and ^{11}C-FEKAP with ^{11}C-GR103545

Figure 5 shows the Guo plots to compare the regional V_T of ^{11}C-EKAP, ^{11}C-FEKAP, and ^{11}C-GR103545. An excellent linear relationship was observed among V_T values across regions, suggesting that the tracers bind to the same target with the same distribution. On the basis of the y-intercepts in Figure 5, ^{11}C-GR103545 has the highest binding potential, followed by ^{11}C-FEKAP and then ^{11}C-EKAP. The regression yielded a negative y-intercept versus ^{11}C-GR103545 (^{11}C-EKAP, −2.41;^{11}C-FEKAP, −0.97). Using the mean population nondisplaceable V_T of ^{11}C-GR103545 (V_{ND}, 3.4 mL/cm^3) and a BP_{ND} range (1.1–7.4) taken from the literature for ^{11}C-GR103545, regional BP_{ND} was estimated to range from 0.6 to 4.3 for ^{11}C-EKAP and from 0.8 to 5.7 for ^{11}C-FEKAP. The ratio of BP_{ND} (^{11}C-EKAP) to BP_{ND} (^{11}C-FEKAP) was 0.75.

DISCUSSION

We evaluated the kinetics of 2 novel KOR agonists, ^{11}C-EKAP and ^{11}C-FEKAP, as PET radiotracers in humans, in comparison with ^{11}C-GR103545, an agonist tracer previously reported by us (*6*).

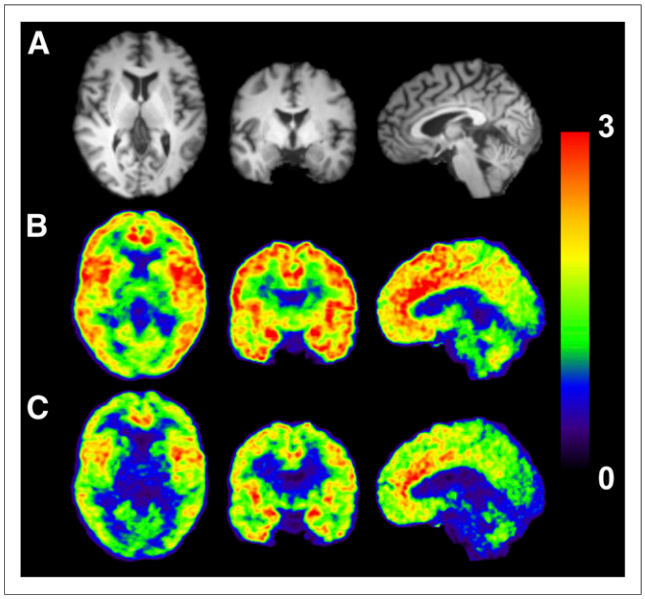

FIGURE 3. Images from typical subject (male, 51 y old, 82-kg body weight). (A) MR images. (B and C) Coregistered PET images summed from 30 to 90 min after injection of ^{11}C-EKAP (B) or ^{11}C-FEKAP (C). SUV is [concentration/(injected dose/body weight)].

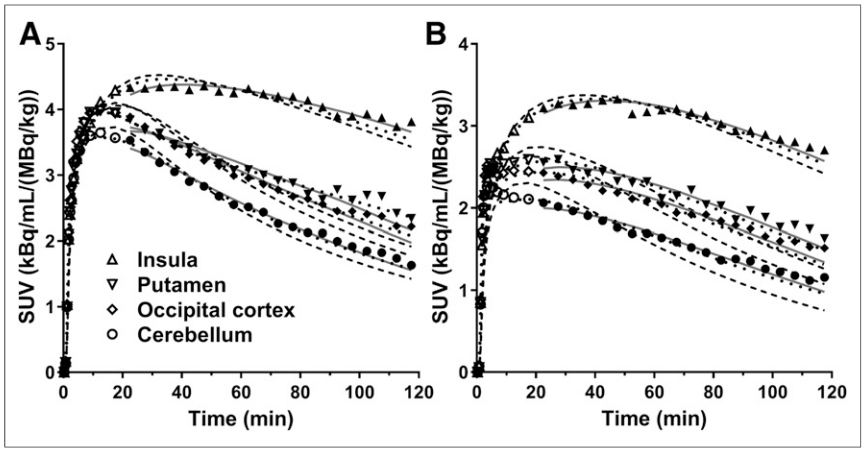

FIGURE 4. Regional time–activity curves in 4 regions of interest after injection of ^{11}C-EKAP (A) and ^{11}C-FEKAP (B) with 1TC (dashed), 2TC (dotted), and MA1 (solid) fits. For each region, symbols correspond to measured regional activity.

Three kinetic models for ^{11}C-EKAP and ^{11}C-FEKAP were compared with arterial input functions. Regional time–activity curves were fitted well by the 2TC model and MA1 for both tracers. V_T was nearly identical between the 2TC model and MA1. As seen for ^{11}C-GR103545 (*6*), the 2TC model produced V_T estimates with large errors in some fits, especially in the amygdala. On the other hand, the MA1 method estimated V_T reliably in all fits and produced similar V_T values for a t^* setting of 10–30 min. For both tracers, MA1 is he model of choice. For the same reason, MA1 (t^* = 40 min) was also selected for ^{11}C-GR103545.

The rank order of V_T and tracer uptake pattern was the same between ^{11}C-EKAP, ^{11}C-FEKAP, and ^{11}C-GR103545. As seen with ^{11}C-GR103545, the thalamus had the lowest V_T for both ^{11}C-EKAP and ^{11}C-FEKAP. For the 1TC K_1 (mL/cm^3/min), ^{11}C-EKAP showed the highest K_1 (0.09–0.21), followed by ^{11}C-GR103545 (0.06–0.14) and ^{11}C-FEKAP (0.033–0.076). For the MA1 V_T (mL/cm^3), ^{11}C-GR103545 (7.3–26.9) gave the highest V_T, followed by ^{11}C-EKAP (5.4–21.6) and ^{11}C-FEKAP (2.3–9.6).

The average TRV (aTRV) of V_T was 7% (range, 4%–17%) for ^{11}C-EKAP, 18% (range, 13%–26%) for ^{11}C-FEKAP, and 15% (range, 8%–41%) for ^{11}C-GR103545. The minimum scan time required for stable V_T estimates was 90, 110, and 140 min for ^{11}C-EKAP, ^{11}C-FEKAP, and ^{11}C-GR103545, respectively. Since these tracers are ^{11}C-labeled, a short scan time (e.g., ≤90 min) is preferred. ^{11}C-FEKAP, with a TRV of more than 15% in most regions, may not be useful for evaluating group differences in receptor availability.

TABLE 2
Regional V_T in Test Scans

	Regional V_T (mL/cm^3)						Minimum scan duration (min)	
	^{11}C-EKAP (n = 6)			^{11}C-FEKAP (n = 6)			^{11}C-EKAP (n = 6)	^{11}C-FEKAP (n = 6)
Region	1TC	2TC	MA1	1TC	2TC	MA1	MA1	MA1
Amygdala	19.9 (22%)	18.1* (6%)	21.6 (25%)	9.1 (33%)	9.0† (39%)	9.6 (36%)	90	90
Insula	13.9 (21%)	14.7 (19%)	15.2 (21%)	6.4 (27%)	6.8‡ (31%)	7.1 (28%)	80	70
Anterior cingulate cortex	13.1 (13%)	13.8 (13%)	14.2 (14%)	5.8 (21%)	6.2 (22%)	6.5 (23%)	70	70
Globus pallidus	10.7 (19%)	11.5 (18%)	11.7 (19%)	4.6 (28%)	5.3 (29%)	5.4 (30%)	70	60
Temporal cortex	9.8 (18%)	11.0 (21%)	10.7 (18%)	4.3 (25%)	4.8 (27%)	5.0 (28%)	80	90
Putamen	9.3 (18%)	10.8 (21%)	10.3 (18%)	3.9 (23%)	4.6 (26%)	4.8 (26%)	80	100
Frontal cortex	9.0 (19%)	10.3 (23%)	9.9 (19%)	4.1 (25%)	4.6 (27%)	4.8 (27%)	80	90
Hippocampus	7.6 (21%)	9.1 (26%)	8.8 (22%)	3.2 (23%)	3.8 (27%)	4.1 (27%)	80	90
Occipital cortex	7.5 (20%)	8.7 (21%)	8.3 (19%)	3.2 (26%)	3.8 (29%)	3.9 (30%)	80	90
Caudate	7.5 (24%)	8.1 (26%)	8.0 (24%)	2.9 (27%)	3.4 (29%)	3.5 (30%)	50	80
Posterior cingulate cortex	6.8 (27%)	7.2‡ (25%)	7.6 (26%)	2.7 (29%)	3.1 (30%)	3.3 (30%)	80	100
Cerebellum	5.7 (32%)	6.6 (29%)	6.4 (29%)	2.1 (34%)	2.6‡ (32%)	3.0 (37%)	80	100
Thalamus	4.8 (20%)	5.2‡ (15%)	5.4 (20%)	1.5 (22%)	1.9‡ (20%)	2.3 (39%)	80	110

*n = 4 (relative SE > 10% was excluded).
†n = 2 (relative SE > 10% was excluded).
‡n = 5 (relative SE > 10% was excluded).
Data in parentheses are percentage coefficient of variation across subjects.

TABLE 3
TRV and Reproducibility of V_T

Region	^{11}C-EKAP			^{11}C-FEKAP		
	aTRV (%)	TRV (%)	ICC	aTRV (%)	TRV (%)	ICC
Amygdala	17 ± 14	4 ± 23	0.19	24 ± 11	−12 ± 26	0.72
Insula	7 ± 6	1 ± 10	0.85	19 ± 9	−5 ± 23	0.63
Anterior cingulate cortex	7 ± 5	3 ± 9	0.78	17 ± 6	−2 ± 20	0.57
Globus pallidus	8 ± 4	2 ± 10	0.82	16 ± 5	−4 ± 18	0.83
Temporal cortex	6 ± 5	0 ± 8	0.91	17 ± 5	−1 ± 20	0.68
Putamen	6 ± 6	−3 ± 9	0.86	13 ± 5	−2 ± 16	0.79
Frontal cortex	5 ± 6	−1 ± 8	0.91	16 ± 5	−3 ± 19	0.71
Hippocampus	5 ± 5	−1 ± 8	0.92	17 ± 7	−5 ± 19	0.72
Occipital cortex	4 ± 5	−1 ± 6	0.96	17 ± 5	−2 ± 19	0.73
Caudate	6 ± 7	−3 ± 9	0.95	17 ± 5	−3 ± 19	0.78
Posterior cingulate cortex	7 ± 6	−1 ± 10	0.95	18 ± 8	−3 ± 21	0.74
Cerebellum	6 ± 5	0 ± 8	0.98	26 ± 14	0 ± 32	0.47
Thalamus	5 ± 7	−2 ± 8	0.87	20 ± 14	3 ± 26	0.55

n = 5/group.

Even though ^{11}C-EKAP showed better reproducibility than the other 2 tracers, the fact that there were a small number of subjects (n = 5) requires a careful interpretation of the test–retest results and numeric values of TRV, aTRV, and ICC. TRV (aTRV = TRV for n = 1) for the excluded subject (whose scans were 69 d apart) was 33% ± 3% for ^{11}C-EKAP and 16% ± 5% for ^{11}C-FEKAP (across regions). This finding indicates that long-term variability in κ-expression might be larger than the TRV reported here. However, more data are required to verify this result.

Since KOR is ubiquitously distributed throughout the brain, there are no appropriate reference regions in humans for use in kinetic modeling, as has been demonstrated in the studies of other KOR agonist and antagonist radiotracers (*3,6*). Therefore, we used the Guo plot to compare the magnitude of nondisplaceable binding potential (BP_{ND}) between the 2 new agonist radiotracers. The linearity of the Guo plot indicates whether the tracers bind with the same target. An almost perfect linear relation was observed between ^{11}C-EKAP and ^{11}C-FEKAP V_T (Fig. 5C), but the linearity between ^{11}C-EKAP or ^{11}C-FEKAP and ^{11}C-GR103545 was not as good (Figs. 5A and 5B). This finding does not necessarily mean that ^{11}C-GR103545 binds to a target different from that of the 2 new tracers, as the results for ^{11}C-EKAP and ^{11}C-FEKAP are from the same group of subjects who received both tracers (whereas those for ^{11}C-GR103545 are not). As there are several regions (e.g., amygdala) with high intrasubject V_T variability, weighting is required to compute the regression line of the Guo plot. We used the inverse of the intersubject SD of V_T as weighting, and we used the total least-squares method to take the intersubject SD of V_T for both tracers into account. The y-intercept of the Guo plot consists of V_{ND} and a ratio of BP_{ND} between the 2 tracers. By substituting the population V_{ND} (3.4 mL/cm^3) and a range of BP_{ND} (1.1–7.4) from ^{11}C-GR103545 into the y-intercept, the BP_{ND} of ^{11}C-EKAP and

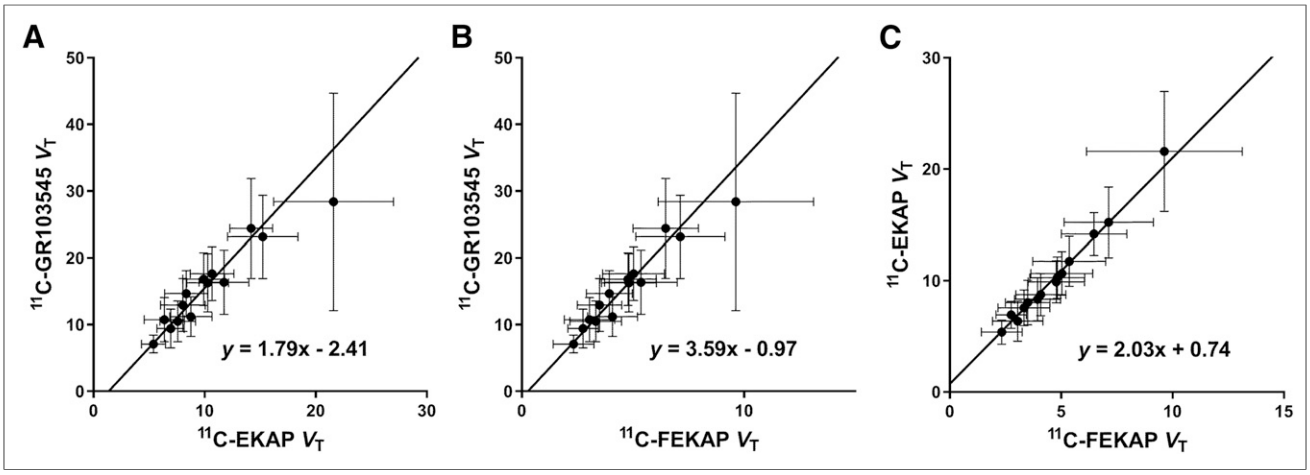

FIGURE 5. Comparisons of V_T for ^{11}C-EKAP, ^{11}C-FEKAP, and ^{11}C-GR103545. Error bars show intersubject variability (SD).

^{11}C-FEKAP can be calculated: the relative binding potentials are 1.71 (BP_{ND} [^{11}C-GR103545]/BP_{ND} [^{11}C-EKAP]) and 1.28 (BP_{ND} [^{11}C-GR103545]/BP_{ND} [^{11}C-FEKAP]). ^{11}C-FEKAP BP_{ND} is similar to ^{11}C-GR103545 BP_{ND}, whereas ^{11}C-EKAP BP_{ND} is lower. Thus, wthe specific binding of ^{11}C-EKAP is predicted to be about 25% lower than that of ^{11}C-FEKAP. The in vivo affinity ratio can be derived from the slope of the Guo plot and the f_P (K_D [^{11}C-EKAP]/K_D [^{11}C-FEKAP] $\approx$ 2). The order of in vitro affinities is inverted (K_D [^{11}C-EKAP]/K_D [^{11}C-FEKAP] = 0.7 (*8,9*)). However, for both in vitro and in vivo studies, a K_D ratio of 2 is unlikely to be significantly different from identity, and it is not uncommon that disparities in in vivo and in vitro affinity measurements are found, because of multiple factors such as measurement temperature, cell or receptor types, and experimental procedures used in vitro.

CONCLUSION

The 2 novel KOR agonist radiotracers ^{11}C-EKAP and ^{11}C-FEKAP display faster kinetic properties than ^{11}C-GR103545. ^{11}C-EKAP displays much better test–retest reproducibility and requires a shorter scan time to obtain stable V_T estimates. Although ^{11}C-EKAP is predicted to have an approximately 25% lower BP_{ND} than ^{11}C-FEKAP, the range of BP_{ND} for ^{11}C-EKAP is very useful (~1–4). Therefore, ^{11}C-EKAP is judged to be a better tracer than ^{11}C-FEKAP for the imaging and quantification of KOR agonist binding in humans.

DISCLOSURE

This study was supported by research grants from the National Institutes of Health (R21MH092664 and R33MH092664). This publication was also made possible by CTSA grant UL1 TR000142 from the National Center for Advancing Translational Sciences (NCATS), a component of the National Institutes of Health (NIH). The contents of this article are solely the responsibility of the authors and do not necessarily represent the official view of NIH. No other potential conflict of interest relevant to this article was reported.

ACKNOWLEDGMENT

We appreciate the excellent technical assistance of the staff at the Yale University PET Center.

KEY POINTS

QUESTION: Which agonist radiotracer shows suitable kinetic properties to quantify KOR in the human brain, ^{11}C-EKAP or ^{11}C-FEKAP?

PERTINENT FINDINGS: The 2 novel KOR agonist tracers show faster tissue kinetics than the current tracer, ^{11}C-GR103545. ^{11}C-EKAP is deemed to be a better tracer for imaging and quantification of KOR, based on the shorter minimum scan time and excellent test–retest reproducibility.

IMPLICATIONS FOR PATIENT CARE: ^{11}C-EKAP shortens the scan time from 140 to 90 min.

REFERENCES

1. Zheng MQ, Nabulsi N, Kim SJ, et al. Synthesis and evaluation of ^{11}C-LY2795050 as a kappa-opioid receptor antagonist radiotracer for PET imaging. *J Nucl Med.* 2013;54:455–463.
2. Ravert HT, Mathews WB, Musachio JL, Scheffel U, Finley P, Dannals RF. [^{11}C]-methyl 4-[(3,4-dichlorophenyl)acetyl]-3-[(1-pyrrolidinyl)-methyl]-1-piperazinecarboxylate ([^{11}C]GR89696): synthesis and in vivo binding to kappa opiate receptors. *Nucl Med Biol.* 1999;26:737–741.
3. Naganawa M, Zheng MQ, Nabulsi N, et al. Kinetic modeling of ^{11}C-LY2795050, a novel antagonist radiotracer for PET imaging of the kappa opioid receptor in humans. *J Cereb Blood Flow Metab.* 2014;34:1818–1825.
4. Naganawa M, Zheng MQ, Henry S, et al. Test-retest reproducibility of binding parameters in humans with ^{11}C-LY2795050, an antagonist PET radiotracer for the kappa opioid receptor. *J Nucl Med.* 2015;56:243–248.
5. Naganawa M, Dickinson GL, Zheng MQ, et al. Receptor occupancy of the kappa-opioid antagonist LY2456302 measured with positron emission tomography and the novel radiotracer ^{11}C-LY2795050. *J Pharmacol Exp Ther.* 2016;356:260–266.
6. Naganawa M, Jacobsen LK, Zheng MQ, et al. Evaluation of the agonist PET radioligand [^{11}C]GR103545 to image kappa opioid receptor in humans: kinetic model selection, test-retest reproducibility and receptor occupancy by the antagonist pf-04455242. *Neuroimage.* 2014;99:69–79.
7. Shalgunov V, van Waarde A, Booij J, Michel MC, Dierckx R, Elsinga PH. Hunting for the high-affinity state of G-protein-coupled receptors with agonist tracers: theoretical and practical considerations for positron emission tomography imaging. *Med Res Rev.* 2019;39:1014–1052.
8. Li S, Zheng MQ, Naganawa M, et al. Development and in vivo evaluation of a kappa-opioid receptor agonist as a PET radiotracer with superior imaging characteristics. *J Nucl Med.* 2019;60:1023–1030.
9. Li S, Zheng MQ, Naganawa M, et al. Novel kappa opioid receptor agonist as improved PET radiotracer: development and in vivo evaluation. *Mol Pharm.* 2019;16:1523–1531.
10. Carson RE, Barker WC, Liow JS, Johnson CA. Design of a motion-compensation OSEM list-mode algorithm for resolution-recovery reconstruction for the HRRT. *IEEE Nucl Sci Symp Conf Rec.* 2003;5:3281–3285.
11. Jin X, Mulnix T, Gallezot JD, Carson RE. Evaluation of motion correction methods in human brain PET imaging: a simulation study based on human motion data. *Med Phys.* 2013;40:102503.
12. Hilton J, Yokoi F, Dannals RF, Ravert HT, Szabo Z, Wong DF. Column-switching HPLC for the analysis of plasma in PET imaging studies. *Nucl Med Biol.* 2000;27:627–630.
13. Tzourio-Mazoyer N, Landeau B, Papathanassiou D, et al. Automated anatomical labeling of activations in SPM using a macroscopic anatomical parcellation of the MNI MRI single-subject brain. *Neuroimage.* 2002;15:273–289.
14. Holmes CJ, Hoge R, Collins L, Woods R, Toga AW, Evans AC. Enhancement of MR images using registration for signal averaging. *J Comput Assist Tomogr.* 1998;22:324–333.
15. Viola P, Wells WM. Alignment by maximization of mutual information. *Int J Comput Vis.* 1997;24:137–154.
16. Papademetris X, Jackowski M, Rajeevan N, Constable RT, Staib LH. Bioimage suite: an integrated medical image analysis suite. *Insight J.* 2006;2006:209.
17. Innis RB, Cunningham VJ, Delforge J, et al. Consensus nomenclature for in vivo imaging of reversibly binding radioligands. *J Cereb Blood Flow Metab.* 2007;27:1533–1539.
18. Ichise M, Toyama H, Innis RB, Carson RE. Strategies to improve neuroreceptor parameter estimation by linear regression analysis. *J Cereb Blood Flow Metab.* 2002;22:1271–1281.
19. Frankle WG, Huang Y, Hwang DR, et al. Comparative evaluation of serotonin transporter radioligands ^{11}C-DASB and ^{11}C-McN 5652 in healthy humans. *J Nucl Med.* 2004;45:682–694.
20. Guo Q, Owen DR, Rabiner EA, Turkheimer FE, Gunn RN. A graphical method to compare the in vivo binding potential of PET radioligands in the absence of a reference region: application to [^{11}C]PBR28 and [^{18}F]PBR111 for TSPO imaging. *J Cereb Blood Flow Metab.* 2014;34:1162–1168.